aerospace

MDPI

Article

Research on Aircraft Attitude Anomaly Auxiliary Decision-Making Method Based on Knowledge Graph and Predictive Model

Zhe Yang [1,2], Senpeng He [2], Yugang Zhang [1,3] and Wenqing Yang [1,3,*]

[1] School of Aeronautics, Northwestern Polytechnical University, Xi'an 710072, China
[2] Chinese Flight Test Establishment, Xi'an 710089, China
[3] National Key Laboratory of Aircraft Configuration Design, Xi'an 710072, China
* Correspondence: yangwenqing@nwpu.edu.cn

Abstract

A knowledge graph is constructed for flight test safety, which is conducive to enhancing the data deduction ability in flight test monitoring and offers efficient and highly complex decision-making support for safety monitoring. Based on this graph, an aircraft attitude predictive model is established by employing neural network technology. This model can accurately predict the changes in aircraft attitude under pilot manipulation, with a mean absolute error of 0.18 degrees in the predicted angle of attack values. By integrating the knowledge graph and the predictive model, an auxiliary decision-making method for abnormal aircraft attitude situations is proposed. This method calculates the safety manipulation space of the aircraft under different flight states through risk quantification technology, providing a theoretical basis for the pilots' manipulation decisions in abnormal attitude situations. The research is verified based on simulation data, which not only enhances the scientific rigor and practicability of flight test safety monitoring in simulated scenarios but also provides new theoretical support and technical approaches for the field of flight safety.

Keywords: knowledge graph; flight test safety; risk quantification; safety manipulation space; auxiliary decision-making

check for updates

Academic Editor: Sybert Stroeve

Received: 28 October 2025
Revised: 11 December 2025
Accepted: 14 December 2025
Published: 18 December 2025

Citation: Yang, Z.; He, S.; Zhang, Y.; Yang, W. Research on Aircraft Attitude Anomaly Auxiliary Decision-Making Method Based on Knowledge Graph and Predictive Model. *Aerospace* **2025**, *12*, 1117. https://doi.org/10.3390/aerospace12121117

Copyright: © 2025 by the authors. Licensee MDPI, Basel, Switzerland. This article is an open access article distributed under the terms and conditions of the Creative Commons Attribution (CC BY) license (https://creativecommons.org/licenses/by/4.0/).

1. Introduction

Flight test is the final stage of aircraft design verification, serving as a critical process to identify, expose, and validate potential design issues. During flight tests, if potential defects are not identified beforehand, the aircraft may otherwise be pushed unintentionally to the edge of its flight envelope, which is extremely challenging and risky. Compared with routine civil operations, flight test conditions involve sparse abnormal samples, strong coupling among subsystems, and limited repeatability of hazardous scenarios. These characteristics significantly constrain the applicability of purely data-driven safety-monitoring approaches and highlight the need for methods that incorporate structured expert knowledge. To enhance situational awareness during abnormal attitude conditions, this study constructs an aircraft attitude prediction model based on the flight test safety knowledge graph, aiming to enable auxiliary decision-making and strengthen the interpretation capability of telemetry data.

In the future, the aviation industry is evolving toward being intelligent, autonomous, distributed, and interconnected, aiming to integrate multiple technologies to ensure flight

safety [1]. Under this development trend, a domain knowledge graph can organically integrate aviation safety knowledge and construct a comprehensive and interrelated knowledge system. The domain knowledge graph [2] focuses on the depth of knowledge, emphasizes the quality of the knowledge base, is constructed using domain-specific data, and has domain-specific significance. It is usually constructed in a top-down approach. From knowledge representation [3,4], knowledge acquisition [5–7], to knowledge fusion [8–10], numerous techniques have been developed to enhance the efficiency and quality of knowledge graph construction.

The rules-based entity extraction method exhibits high accuracy but low efficiency. Consequently, deep-learning-based approaches have been widely explored. Xiong M et al. apply the Bi-LSTM-CRF method [11] to extract deeply embedded security-related entities from civil aviation accident texts.

The research on the combination of Large Language Model (LLM) and knowledge graph shows promise [12–14]. Dagdelen J et al. have utilized LLM [15] to automatically extract knowledge from unstructured texts. Qu J et al. [16] have proposed a remote supervised relationship extraction method based on reinforcement learning for clustering to extract the relationships between aviation accident entities. Currently, graphs are mostly applied in intelligent question answering [17,18], recommendation systems [19], and knowledge visualization [20]. This type of application requires a breadth of knowledge; however, they often lack depth and may introduce duplication of identical knowledge, irrelevant knowledge, and erroneous knowledge when dealing with heterogeneous data sources.

Main approaches include data-based auxiliary decision-making [21], model-based auxiliary decision-making [22,23], and knowledge graph-based auxiliary decision-making [24]. These three approaches provide different perspectives and methods for solving complex decision-making problems. Many studies combine two or three of them to conduct research on auxiliary decision-making. For instance, safety alarm issues have been studied based on model-based and data-based frameworks [25,26].

Alarm information is the key input for flight test safety-auxiliary decision-making. Through the analysis of alarm information and the security risk quantification methods [27,28], the degree of security risk in the current flight test state can be assessed, and data-driven methods combined with feature extraction can further improve the accuracy of risk-related parameter prediction [29]. Aviation safety risks have been evaluated based on flight data and pilot behavior characteristics [30], specifically, pilot behavior can affect the response to risks such as take-off runway overrun [31,32] and flight in icy conditions [33], but not the occurrence of these events. Risk quantification aims to clarify the dangerous state, determine the dangerous state, and explore how to restore the safe state. The problem of stalling has been studied by planning flight paths [34], minimizing the loss of altitude [35], or adopting flow control technologies such as plasma actuators to delay stall occurrence [36].

Building on these insights, this study introduces the principles of auxiliary decision-making, analyzes the relationships among the flight test safety knowledge graph, prediction model, decision, and support system, and proposes a linear risk quantification method. The safe maneuvering space calculation, knowledge graph design, visualization, and the neural-network-based attitude prediction model are presented. Finally, the framework's effectiveness is validated using angle-of-attack and sideslip-angle examples.

2. The Auxiliary Decision-Making Method Based on Knowledge Graph and Predictive Model

2.1. Principle of Auxiliary Decision-Making

To provide support for unexpected situations during flight, the auxiliary decision-making should be clear about two goals: one is to improve the decision-making efficiency,

that is, to push the most accurate decision-making information at the fastest speed when unexpected situations occur. With the knowledge graph as the basic tool, telemetry data are combined with flight safety knowledge, enabling alarm information and disposal measures to be quickly pushed when relevant parameters meet the alarm discrimination requirements. The other goal is to enhance the analysis ability of complex faults. For complex faults encountered during flight tests, it is necessary to be able to identify the essence, analyze the key alarm causes and solutions from a large amount of data, and provide a strong theoretical support for auxiliary decision-making.

The principle of the auxiliary decision-making is illustrated in Figure 1. The auxiliary decision-making system primarily comprises the knowledge graph of flight test safety, the flight test safety model, and the auxiliary decision-making model.

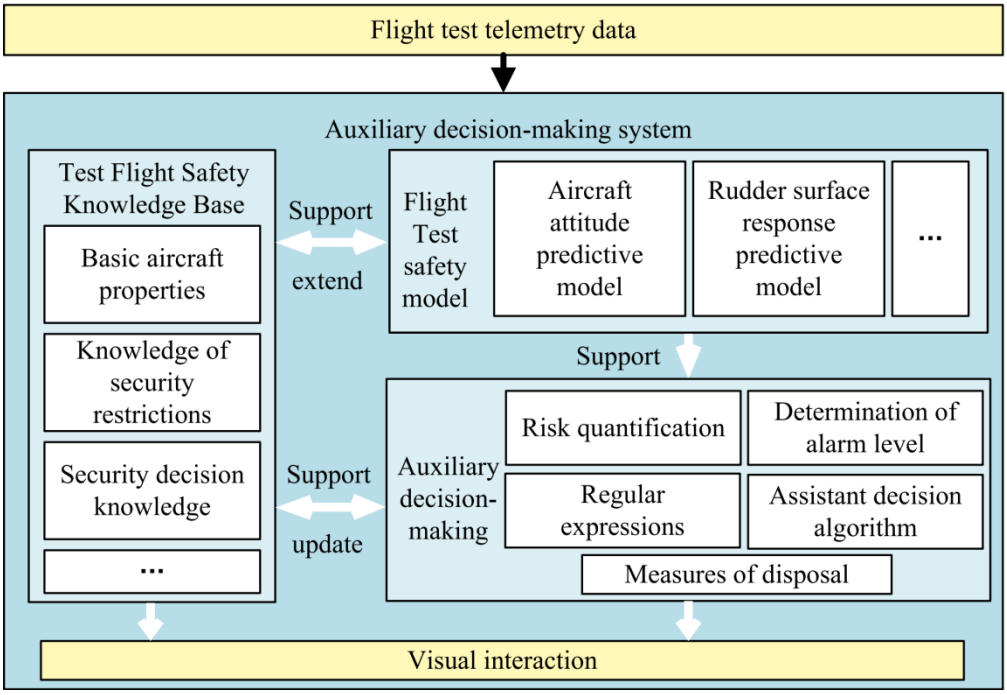


Figure 1. The principle of assisted decision-making.

The knowledge graph of flight test safety includes basic aircraft attributes, knowledge of security restrictions, and security decision knowledge. This knowledge provides support for the construction of flight test safety models and auxiliary decision-making models. Flight test safety monitoring personnel can quickly query the concerned and related safety knowledge through the knowledge graph.

The flight test safety model serves a specific role. It does not directly participate in decision-making. Instead, it integrates flight test safety knowledge. It extracts numerous parameters from the obtained flight test telemetry data. Then, through calculations, it simplifies the multi-dimensional parameters to obtain the parameters required by the reduced dimensional auxiliary decision-making model. This process is also the process in which commanders and ground engineers analyze and process numerous data when making auxiliary decisions.

The auxiliary decision-making model mainly includes risk quantification, determination of alarm levels, and assistant decision algorithms. By integrating knowledge graphs and flight test safety models, the auxiliary decision-making model quantifies risks and determines alarm levels for key safety parameters, thereby clarifying the importance of the alarm items to be addressed. Then, it associates the warning items with handling measures through regular expressions or auxiliary decision-making algorithms. Finally,

it presents the handling measures through visual interaction to provide decision support. Good decision-making cases can be stored in the knowledge base to update the flight test safety knowledge graph. This study conducts preliminary exploration based on simulation scenarios, providing technical reference for subsequent applications in real flight tests.

The construction of auxiliary decision system is a gradual development process. The auxiliary decision method for the aircraft attitude anomaly problem is mainly studied, providing reference for other flight test safety problems where the knowledge graph and model are utilized for auxiliary decision making. The aircraft attitude predictive model is used to calculate the predicted values of aircraft attitude parameters, and the safety range of aircraft attitude is defined by combining the knowledge graph. The risk value is calculated by the risk quantification method, and then the safety manipulation space is determined. The alarm information was associated with the disposal measures in the flight manual, and the decision suggestions could be pushed in time when the alarm occurred, so as to improve the decision-making efficiency and ensure the safety of the test flight. In the following, the risk quantification method of aircraft attitude parameters and the construction of safety manipulation space model are mainly introduced.

On this basis, a human-in-the-loop extended closed-loop framework is established in Figure 2. It is important to emphasize that this framework functions as an external supervisory decision-support system, primarily assisting ground monitoring personnel in assessing abnormal conditions and selecting appropriate response measures. The framework does not intervene in or modify the onboard closed-loop stability augmentation system (e.g., SAS), nor does it assume control authority over the aircraft. Instead, it provides predictive trends, risk assessments, and recommended actions as advisory information. Flight crew or ground personnel may choose whether to adopt these suggestions, and multiple valid recovery strategies may exist for the same abnormal condition. This separation ensures that the auxiliary system improves situational awareness and decision-making efficiency without interfering with the aircraft's inherent stability control loops.

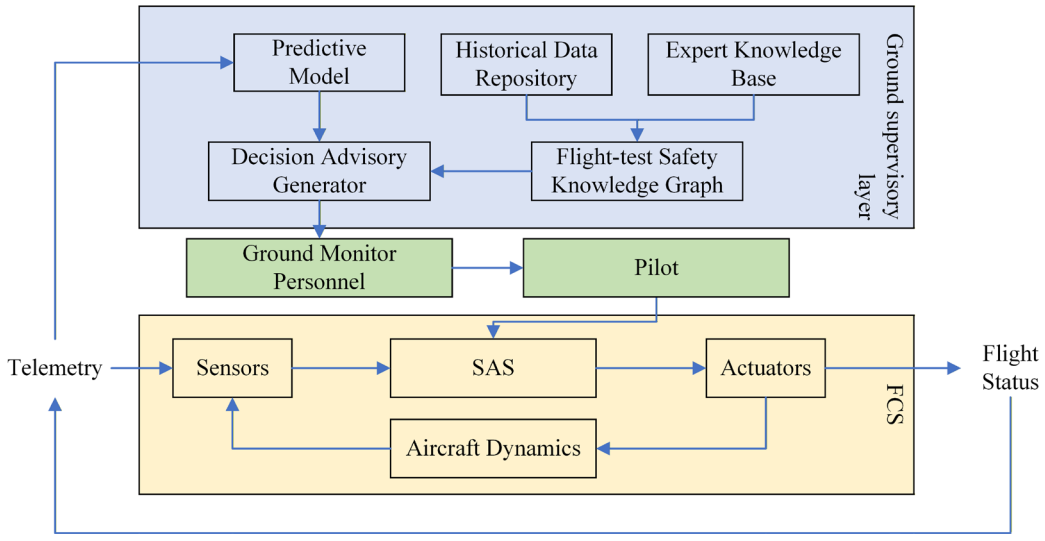


Figure 2. Closed-loop control architecture.

2.2. Risk Quantification Methods

Aircraft attitude anomaly is one of the important threats to flight safety. From the perspective of aircraft simulation telemetry data, aircraft attitude anomaly is often reflected in the anomaly of key parameters such as aircraft attitude angle, aircraft attitude angle change rate, acceleration, airspeed, or flight trajectory. However, how many of these parameters count as abnormal is different for different aircraft and different flight tasks,

and how to evaluate whether the current aircraft attitude parameters are normal is the prerequisite for decision-making.

The existing safety assessment methods are based on observing whether the real-time critical telemetry parameters of the aircraft exceed the safety limit value, and the cognition of the parameter limit is vague. For instance, the angle of attack limit is set at 16 degrees, but an angle of attack exceeding 15.5 degrees is equally dangerous. To quantify this restriction, many studies divide the parameter limit value into multiple segments and give the risk value or risk level by means of intervals. However, the improvement or reduction in the risk level can only be perceived at the abrupt change in the interval, and the increase or decrease in the parameter value in the interval cannot be perceived.

To address this issue, the risk value is designed as a piecewise linear function of the parameter limit interval. For instance, if the design limit interval of a key safety parameter x is [x_0, x_1], the r_1% and r_2% of the design limit interval are taken as the two risk levels of this parameter. The risk level intervals of the parameter value can be divided into seven intervals based on x_0, x_1, x_{0r1}, x_{0r2}, x_{1r1}, and x_{1r2}. The risk value range of different intervals is set within [1, 8]. Then, the calculation formula of the risk value for this parameter is given by Equation (1).

$$R = \begin{cases} 8 & (x < x_0) \\ 2 + 6\frac{x - x_0}{x_{0r2} - x_0} & (x_0 < x < x_{0r2}) \\ 1 + \frac{x - x_{0r2}}{x_{0r1} - x_{0r2}} & (x_{0r2} < x < x_{0r1}) \\ 1 & (x_{0r1} < x < x_{1r1}) \\ 1 + \frac{x - x_{1r1}}{x_{1r2} - x_{1r1}} & (x_{1r1} < x < x_{1r2}) \\ 2 + 6\frac{x - x_{1r2}}{x_1 - x_{1r2}} & (x_{1r2} < x < x_1) \\ 8 & (x > x_1) \end{cases} \tag{1}$$

In this context x_{0r1}, x_{0r2}, x_{1r1}, and x_{1r2} are assumed to be functions of x_0, x_1, r_1%, and r_2%, respectively, as seen in Equation (2).

$$\left.\begin{array}{l} x_{0r1} = \frac{x_0 + x_1}{2} - \frac{x_1 - x_0}{2} \cdot r_1\% \\ x_{0r2} = \frac{x_0 + x_1}{2} - \frac{x_1 - x_0}{2} \cdot r_2\% \\ x_{1r1} = \frac{x_0 + x_1}{2} + \frac{x_1 - x_0}{2} \cdot r_1\% \\ x_{1r2} = \frac{x_0 + x_1}{2} + \frac{x_1 - x_0}{2} \cdot r_2\% \end{array}\right\} \tag{2}$$

According to the calculation formula, the change curve of risk value with parameter value is drawn in Figure 3. When the risk value is 1, it means that the parameter is within the normal range, and when the risk value is equal to 8, it means that the current parameter is seriously exceeded. How to define the interval in the formula can be adjusted according to the flight test task and the safety monitoring task.

Taking angle of attack as an example, according to the design safety knowledge stored in the knowledge graph, the angle of attack limit of C172P aircraft is $(-5, 16)$ degrees, and the percentage of risk level interval is set as 80% and 90%. According to the formula, the change curve of angle of attack risk value with angle of attack can be obtained in Figure 4. On the left side, the risk value is determined according to the parameter interval, and the risk value in the interval is constant. On the right side, the risk value is calculated by linear interpolation, and the parameter can also be identified when the parameter changes in the interval.

When the two risk quantification methods were applied to quantify the risk of angle of attack in a certain period of time during a flight, the results were obtained in Figure 4, and the applied risk quantification methods corresponded to Figure 4. It can be seen from Figure 5 that when the linear interpolation method is used to calculate the risk value

of the parameter, the change in the risk value with the parameter can be more clearly perceived. For example, the right figure shows that the risk value of the angle of attack tends to decrease with the pilot's control at about 80–100 s, while the left risk value figure cannot perceive the change. The risk value on the right side can be clearly seen at which moment the risk value is the largest, and the change in the risk value can also be clearly perceived. The risk value contains more key information, which is more conducive to the safety monitoring personnel to make auxiliary decisions.

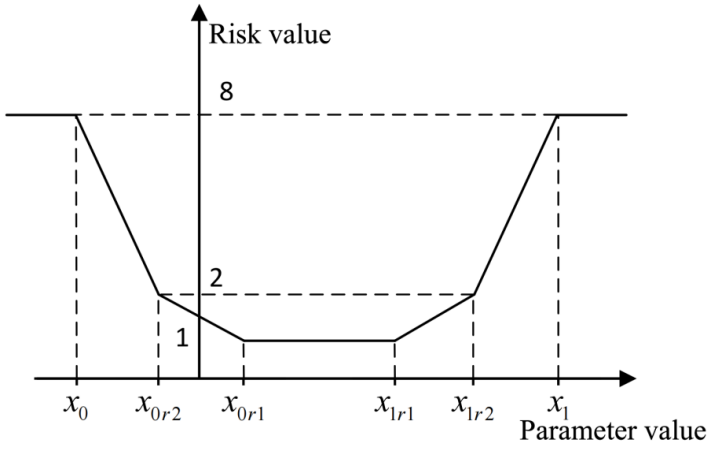


Figure 3. Risk quantification curve.

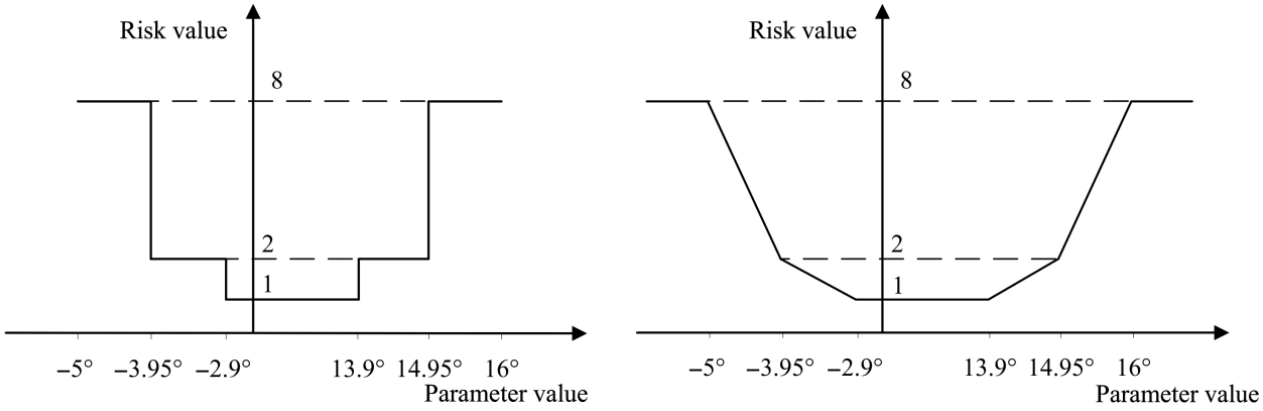


Figure 4. Comparison of risk quantification curves.

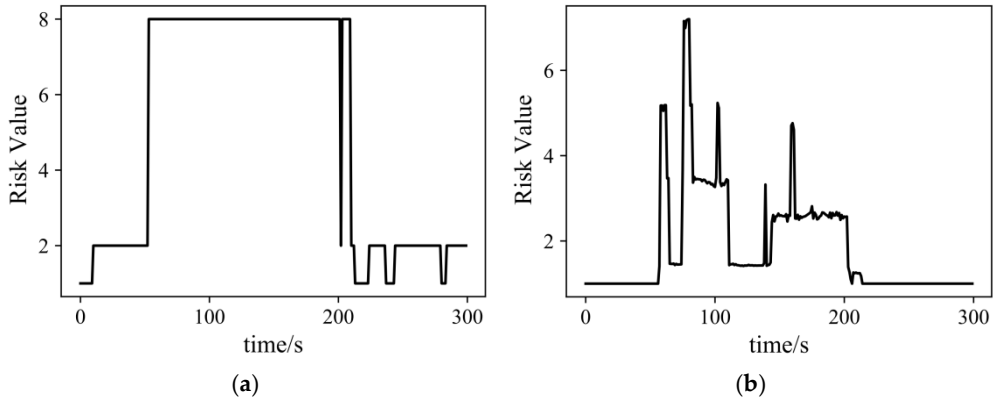


Figure 5. Comparison of angle of attack risk curves under different quantification methods: (**a**) quantitative methods for risk range; (**b**) quantitative methods for risk linearity.

The risk quantification can only represent the dangerous state of the aircraft and cannot give specific decision-making suggestions. In the following, the risk quantification method is combined with the aircraft attitude predictive model to calculate the aircraft safety manipulation space, so as to provide theoretical support for decision-making.

2.3. Construction of Safety Manipulation Space Model

The quantitative method of aircraft attitude anomaly risk can evaluate the real-time safety of flight. However, this method has obvious limitations in predicting the change trend of key safety parameters in the future. In order to improve the predictive accuracy of the change trend of key safety parameters, an aircraft attitude predictive model is constructed to predict the aircraft's key attitude parameters. The prediction accuracy of this model is more accurate and reliable than that of the observation method.

In the actual flight, when the parameters exceed the limit, it is often accompanied by the anomaly of multiple related parameters. Therefore, it is not only necessary to consider the real-time overrun parameters of the aircraft, but also to identify the potential overrun parameters and calculate the predictive value combined with the predictive model and then calculate the risk to predict other possible overrun parameters.

By constructing the aircraft safety manipulation space model shown in Figure 6, the flight test safety knowledge graph, aircraft attitude predictive model, and risk quantification method are combined to enhance the parameter risk perception ability and improve the efficiency and accuracy of auxiliary decision-making. In the aircraft safety manipulation space model, the target monitoring parameters are first determined, and two manipulation parameters that have an impact on the target monitoring parameters are selected. At the same time, the simulation telemetry data is received to determine the input data matrix. The data is input into the aircraft attitude predictive model to obtain the target monitoring parameter value matrix, and then the risk value of the target parameter value matrix is calculated by the risk quantification method. The parameters required by the aircraft attitude predictive model and the target parameter thresholds required by the risk quantification method are obtained from the flight test safety knowledge graph. After drawing the calculated risk value as the target parameter prediction risk heat map in the manipulation space, the specific aircraft safety manipulation space can be determined according to the risk threshold in the flight test safety knowledge graph, and the pilot control advice can be given combined with the aircraft safety manipulation space.

The aircraft manipulation space here mainly considers the control range of the throttle and the main control surfaces, which refer to the elevator, rudder, and left aileron (the deflection angles of the left and right ailerons are of the same size but in opposite directions). The left aileron deflects downward as positive, and the aircraft rolls to the right; if the rudder deflects to the left as positive, the aircraft will yaw to the left, and the elevator tilts downward as positive, and the aircraft bows down. In addition, the gas is closely related to the aircraft's flight performance and maneuverability. The throttle is included in the discussion of the aircraft's space, and a more comprehensive understanding of the aircraft's flight characteristics and maneuverability is achieved.

In the specific implementation, the aircraft attitude parameters mainly focus on the angle of attack, sideslip angle, roll angle, and pitch angle. When the angle of attack and pitch angle are concerned, the throttle and elevator are usually mainly chosen as the control parameters. When the sideslip angle and roll angle are concerned, the aileron and rudder are usually the primary control parameters. Taking angle of attack overrun and sideslip overrun as examples, the safety manipulation space model is applied to study the auxiliary decision-making.

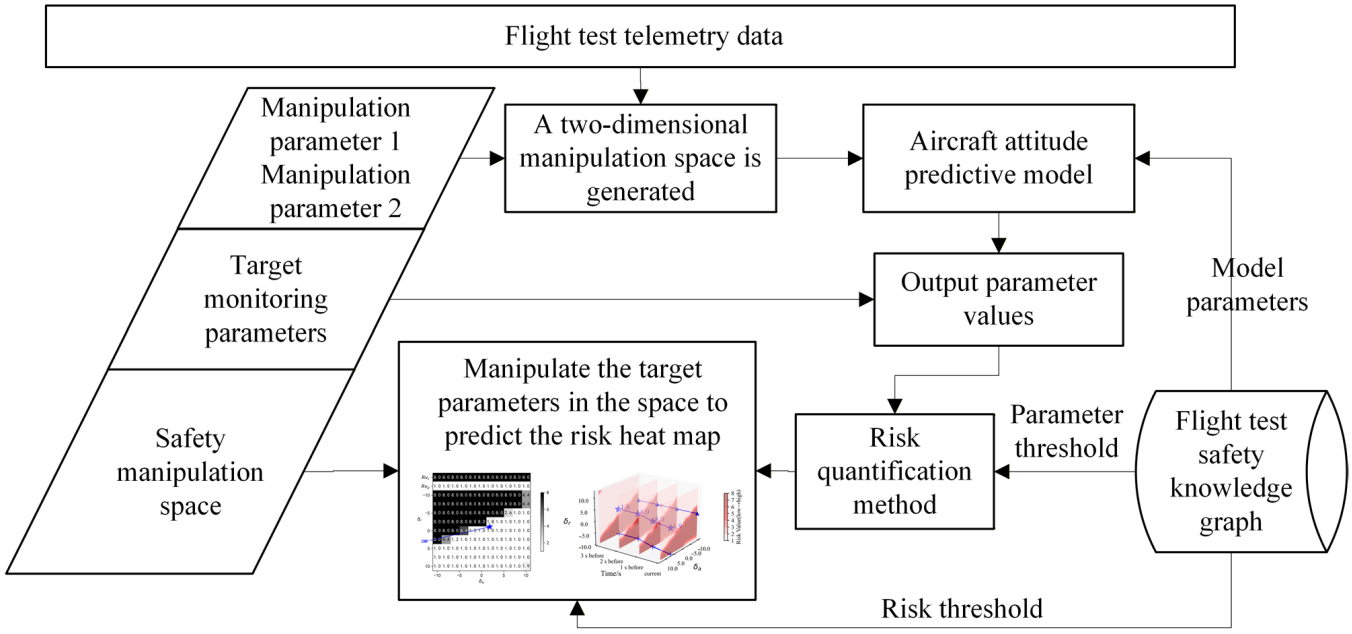


Figure 6. Safety manipulation space model.

3. Construction of Flight Test Safety Knowledge Graph

3.1. Conceptual Model of Knowledge Graph

The conceptual model of knowledge graph is divided into ontology layer and instance layer. The ontology layer is composed of entity types and their attributes, relationship types between entity types, rules and other ontology-related knowledge elements. The instance layer is the instantiation of the ontology layer, which is composed of the entities, attributes, relations, and other knowledge elements corresponding to the entity type. The core of the knowledge graph is the entity, which represents the specific object in the flight test safety. The entity type is the classification of these entities, and each entity type can be regarded as a broader category; that is to say, the ontology layer and the instance layer are relative. In different levels of the graph, the entities may belong to the ontology layer or the instance layer.

Concept graph knowledge model, as shown in Figure 7, according to the ontology layer structure, builds instance layer. Attributes are specific descriptions of entities, providing detailed information about the entity. Attributes can help distinguish different entities with similar characteristics and enhance the semantic understanding of entities. For example, for an aircraft entity, its attributes might include basic aircraft information, aircraft geometric dimensions, engine system, etc. For an engine fuel system entity, the attributes might include the amount of fuel remaining, fuel consumption rate, fuel density, etc.

After understanding the entities, relationships, and attributes of the conceptual model of the knowledge graph, the following introduces how to construct the flight test safety knowledge graph through examples, and visualizes it with the Neo4j development tool Neo4j Browser (version 4.4, LTS).

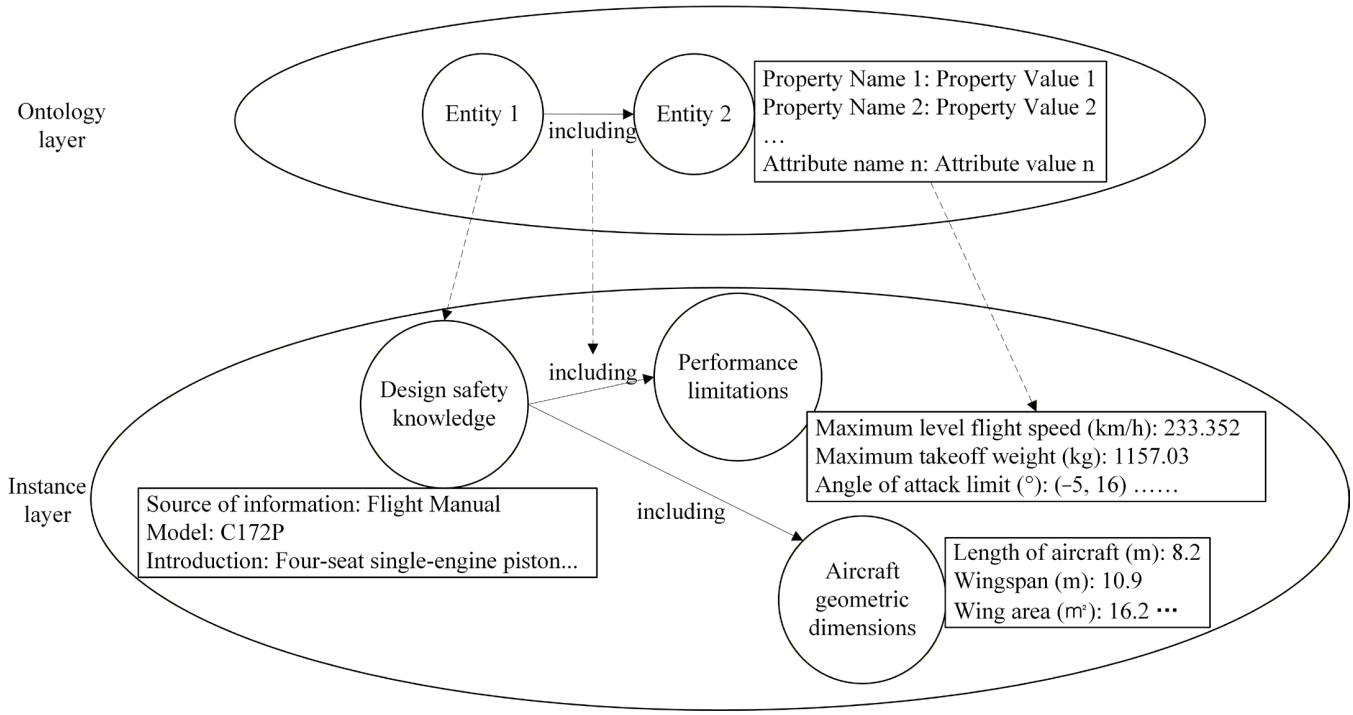


Figure 7. Conceptual model of the knowledge graph.

3.2. Examples and Visualization of the Flight Test Safety Knowledge Graph

3.2.1. Knowledge Graph of Aircraft Basic Attributes

When constructing the knowledge graph for flight test safety, the basic attribute knowledge of the aircraft is a core component. The basic attribute knowledge of aircraft mainly comes from flight manuals and other sources, and it belongs to design safety knowledge. During the knowledge extraction process, Table 1 is used for extraction.

Table 1. Knowledge extraction table of basic attributes of aircraft.

Node	Knowledge Sources	Attribute Name 1	Attribute Parameter 1	Attribute Name 2	Attribute Parameter 2	Attribute Name 3	Attribute Parameter 3
Basic aircraft information	Flight manual	Aircraft name	C172P	Introduction	light general aircraft	service ceiling	4271.2 m
Aircraft geometric dimensions	Flight manual	Captain	8.2 m	Wingspan	10.9 m	Wing area	16.2 m^2
Engine system	Flight manual	Model of engine	eng_io320	Model of propeller	prop_75in2f	Diameter of the propeller	1.91 m

Aircraft geometry and mass properties: These properties (directly or indirectly measurable) include dimensional information: empty weight, product of inertia, moment of inertia, wingspan, and wing area; such data is crucial for understanding the aircraft's physical characteristics and flight performance.

Engine system: It encompasses core parameters: engine model, engine type, engine thrust, fuel mass, fuel tank location, installation angle, engine bypass ratio, and fuel consumption rate; these parameters are critical for evaluating the aircraft's power performance and fuel efficiency.

Flight control system: It involves key functional indicators: response range of aircraft control surfaces and mapping relationship between control inputs and system responses; this knowledge assists pilots and engineers in understanding attitude/heading control via the flight control system.

Aerodynamic performance: It includes aerodynamic coefficients: lift coefficient (lift aerodynamic derivative), drag coefficient, pitching moment coefficient, side force coefficient, rolling moment coefficient, and yawing moment coefficient; these parameters are essential for analyzing aerodynamic behavior under different flight conditions.

Environmental knowledge: It covers basic model-building parameters: air density, gravitational acceleration, and terrain data; these parameters are stored in the flight test safety knowledge graph and are vital for predicting performance under various environmental conditions.

The knowledge extraction table of the basic attributes of the aircraft is converted into a knowledge graph as shown in Figure 8. Through this graph, users can easily retrieve the basic attributes of the aircraft. Simply by clicking on the corresponding node, they can quickly access detailed information. For example, by clicking on the plane for basic information, they can quickly see key properties such as the plane name, introduction, service ceiling, the maximum level flight speed, maximum take-off weight, and angle of attack limit.

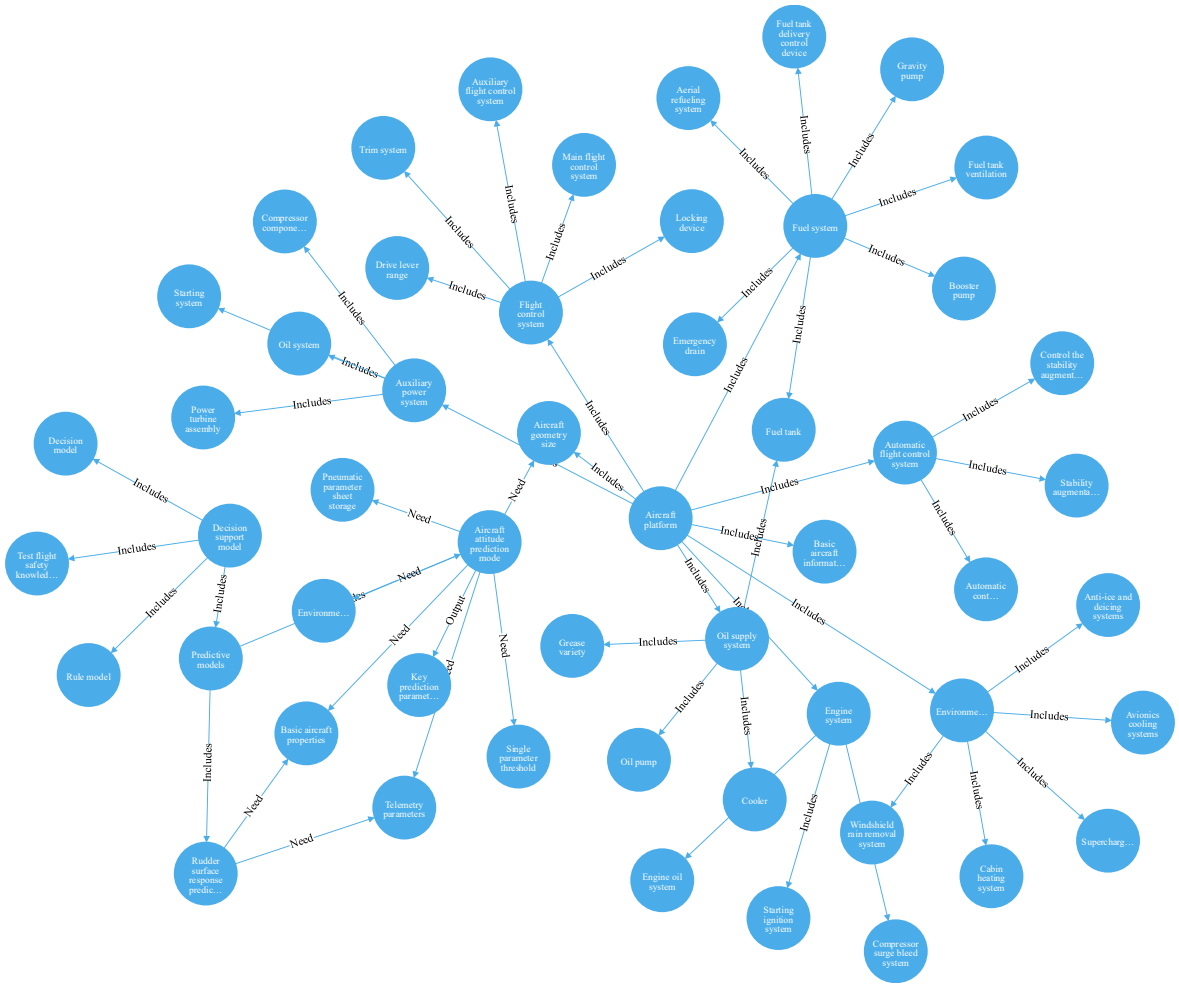


Figure 8. Schematic of knowledge graph for aircraft basic attribute.

3.2.2. Knowledge Graph of Aircraft Attitude Predictive Model

The flight test safety knowledge extraction table required by the aircraft attitude predictive model is similar to the knowledge extraction table of the basic attributes of the aircraft, which is omitted here. The safety knowledge related to the aircraft attitude predictive model can be converted into the knowledge graph, and Figure 9 can be obtained. The figure demonstrates that the input parameters for training the aircraft attitude

prediction model primarily consist of manipulation parameters, attitude parameters, and state parameters, all of which are derived from the dataset. During model training and flight safety monitoring, the input parameters come from simulation telemetry data. The output of the model is the key prediction parameter. The theoretical methods used in the model include correlation analysis and neural networks. Alarm model requires the aircraft attitude predictive model. The aircraft attitude predictive model belongs to the predictive model for auxiliary decision-making. The attributes of the control parameters input to the model mainly include lateral control, longitudinal control, and power control.

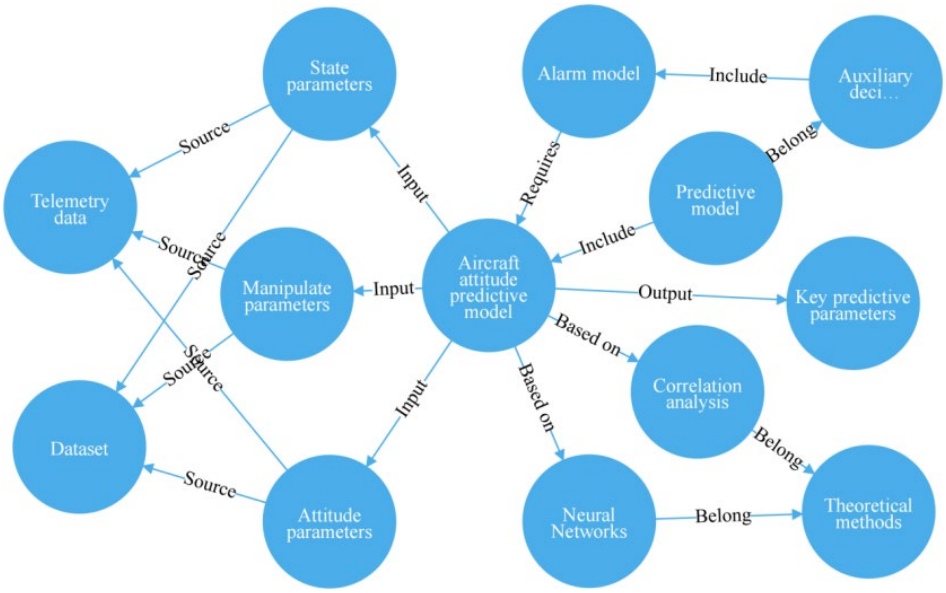


Figure 9. Schematic of knowledge graph for model.

Knowledge graph can help flight test engineers understand the input and output of the model, quickly locate different data sources, and help flight test engineers maintain the model through knowledge graph analysis.

To avoid introducing uncertainty during flight tests, the knowledge graph employed in this paper is a stable version validated by experts, which does not undergo real-time dynamic updates during actual decision support. Interaction between the knowledge graph and learning modules follows a post-flight offline update model: after flight completion, telemetry data undergoes integrity checks, noise processing, and validity verification. Subsequently, the learning module utilizes this validated data to update predictive models or relationships within the graph. Updated content must pass rule checks or expert review before generating a new reliable version for subsequent flight missions.

3.2.3. Knowledge Graph of Auxiliary Decision

Auxiliary decision knowledge is the key to determining the threshold value of parameters. Parameter thresholds can be determined from two aspects: design knowledge and empirical knowledge. The design knowledge is derived from the flight manual, and the traditional flight envelope concept is usually used for aerodynamic variables (angle of attack, altitude, speed, center of gravity, etc.), which represents the available threshold for normal plane flight. The upper/lower limit threshold is usually defined according to the aerodynamic characteristics of the aircraft and the structure durability. Using these restrictions as alarm thresholds can ensure safe manipulation within the scope of the design plane.

Empirical knowledge first needs to be obtained through characteristic analysis and in combination with flight manuals, standards, and knowledge of expert experience to clearly associate flight parameters with the flight safety state. The key state parameters include the angle of attack, sideslip angle, speed, pitch angle, roll angle, pitching angle speed, yaw angular velocity, normal overload, falling velocity, etc. These parameters describe the plane's spatial location, direction, and dynamic characteristics.

Based on the empirical knowledge, setting the alarm threshold is more practical and reliable. With the passage of time and the accumulation of flight data, it can be continuously updated to reduce unnecessary alarms. This method is more conservative because it is based on the worst historical data and can ensure that even in extreme cases, it is not beyond the scope of security. Based on design knowledge and experience, the key threshold parameters for safety attitude are extracted in Table 2.

Table 2. Thresholds of key safety attitude parameters.

Nodes	Property Name 1	Attribute Parameter 1	Attribute Name 2	Attribute Parameter 2
Angle of attack over the upper limit	Design safety limits	Angle of attack greater than 16°	Empirical safety knowledge	-
Angle of attack over the lower limit	Design safety limits	Angle of attack less than −5°	Empirical safety knowledge	-
sideslip angle over the upper limit	Design safety limits	-	Empirical safety knowledge	Sideslip angle greater than 8°
sideslip angle over the lower limit	Design safety limits	-	Empirical safety knowledge	Sideslip angle less than −5°

The knowledge and decision information required for auxiliary decision-making are stored in the corresponding alarm node as shown in Figure 10. Click the alarm node of the over-upper-limit of the angle of attack to view the attributes. The parameters that need to be considered during the alarm include the angle of attack, the sideslip angle, the elevator, and the throttle, etc. In the judgment of the alarm, the angle of attack is more than 16°. The handling advice is to deflect the elevator downward for the pushrod while coordinating the reduction in the throttle. The main sources of knowledge for this alarm are flight manuals, risk quantification methods, and aircraft attitude predictive models. The limits specified for the angle of attack are [−5, 16] degrees.

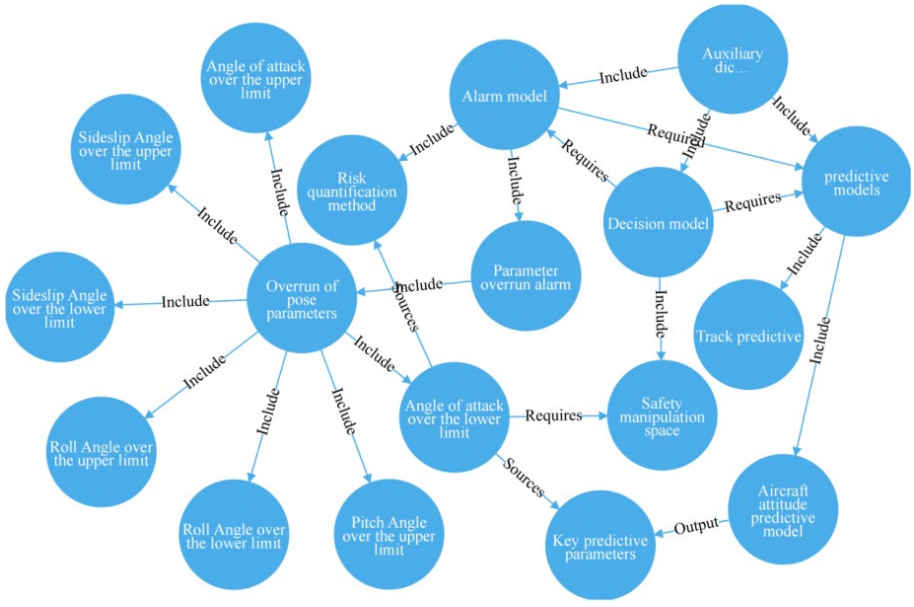


Figure 10. Schematic of knowledge graph for auxiliary decision-making.

On the one hand, the output of the aircraft attitude predictive model provides the predicted value of the angle of attack; on the other hand, the risk quantification method of the alarm model and the parameter overrun alarm give the criterion of the angle of attack value exceeding the limit, and jointly determine that the angle of attack is over the upper limit. The safety manipulation space available after the angle of attack exceeds the limit provides theoretical support for the suggestions on control put forward by the auxiliary decision-making model.

4. Aircraft Attitude Predictive Model Construction

4.1. Data Analysis and Model Parameter Design

Based on the six-degree-of-freedom calculation equation of the aircraft, the parameters that may affect the aircraft's attitude were analyzed. The flight gear was used to obtain simulation data, which is based on the JSBSim open-source simulation program. Referring to the actual data reception frequency of safety monitoring, the data reception frequency during the simulation flight was set at 8 Hz, and a total of 50,710 data points were obtained. The influence of ground effect on the aircraft's attitude is not considered, and thus the simulation flight data with an altitude of over 100 m (the airport altitude is 45 m) was selected. Overall, 80% of the data, a total of 40,568 data points, were taken as the train set, and 20%, a total of 10,142 data points, were taken as the test set.

The Pearson coefficient was calculated using the obtained simulation data and a heatmap was drawn as shown in Figure 11. In the figure, u, v, w, p, q, and r represent the velocity and angular velocity of the aircraft in the body coordinate system in three directions, respectively. Additionally, t and $t+1$ represent the current moment and the moment 1 s later, respectively. This 1 s prediction horizon corresponds to eight steps ahead because the telemetry sampling rate is 8 Hz (0.125 s per frame). Moreover, the parameters α, β, ϕ, θ, h, δ_a, δ_e, δ_r, δ_t, δ_f, and n_p represent the angle of attack, sideslip angle, roll angle, pitch angle, altitude, aileron deflection, elevator deflection, rudder deflection, throttle, flap deflection, and engine speed, respectively. The figure clearly shows the correlation between these key flight parameters and the aircraft attitude variables (including angle of attack, sideslip angle, roll angle, and pitch angle). For example, the rudder and sideslip angle show a strong positive correlation (correlation coefficient of 0.79), and the elevator and angle of attack (correlation coefficient of -0.87) and the elevator and pitch angle (correlation coefficient of -0.51) show a strong negative correlation. The correlation between the flap and the attitude angle is relatively low, so the flap parameter is removed when building the model to reduce the impact of unnecessary parameters on the results.

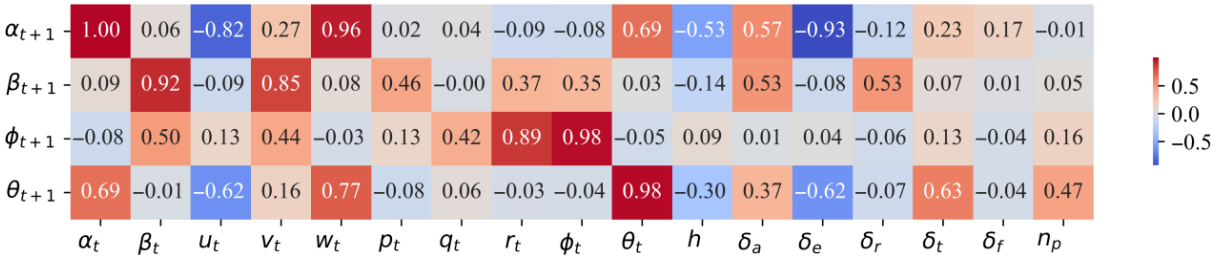


Figure 11. Heat map of Pearson coefficients between input parameters and key attitude parameters of the aircraft.

After determining the parameters required for the model, the dataset is organized and input into the neural networks for training. The input layer receives data with 16 feature dimensions, which then undergoes feature transformation through the hidden layer, and finally, the output layer generates four predictive results. The selection of the network

structure and hyperparameters is a complex process. As shown in Table 3, there are a total of 81 combinations of hyperparameters. Here, GridSearchCV implemented in scikit-learn (version 1.2.2) is applied for parameter tuning. GridSearchCV can automatically search for the best parameter combination through grid search, reducing the workload of manual parameter adjustment and improving model performance. In this process, GridSearchCV is employed to perform five-fold cross-validation. Each parameter combination is trained and tested five times, with different training and test sets utilized each time. The average value of the negative mean squared error in the five tests is used as the quantitative standard for finding the optimal parameter combination.

Table 3. Hidden layer structure and hyperparameter design.

Parameter Names	Set Range	Optimal Parameter Settings
Hidden layer structure	(128), (256 64), (256 128 64)	(256 128 64)
L2 regularization factor	0.01, 0.05, 0.1	0.01
Initial learning rate	0.1, 0.01, 0.001	0.001
Maximum number of iterations	100, 400, 1000	100

To prevent the model from overfitting, L2 regularization was introduced during training. Specifically, the regularization term calculates the sum of squared L2-norms of all weight parameters in the model, and the coefficient is set to 0.01 to balance the weight of the regularization term and the original loss function in the total loss. The original loss function is based on the mean square error (MSE) loss, evaluation model prediction, and the difference between the observed value. In terms of the optimization algorithm, this model uses the Adam optimizer, which combines the advantages of RMSprop and Momentum algorithms, and can adaptively adjust the learning rate to adapt to the optimization needs of different parameters.

4.2. Analysis of Model Training Results

As shown in Table 4, the model training results were evaluated using mean squared error (MSE), mean absolute error (MAE), and coefficient of determination (R^2), all of which were greater than 0.9, indicating a good fit of the model to the training set. The MAE of the roll angle was 0.923 and the MSE was 2.001, suggesting slightly lower accuracy and stability.

Table 4. Evaluation metrics for model training results.

Evaluation Metrics	α	β	φ	θ
MSE	0.070	0.160	2.001	0.506
MAE	0.144	0.280	0.923	0.456
R^2	0.991	0.924	0.975	0.991

The results of the model training are shown in Figure 12. The left side is the time series curve of the actual values and predicted values, and the right side is the scatter plot of the actual values and predicted values. There are deviations near the extreme points on the time series curve. The fitting effect of the sideslip angle in the scatter plot is slightly poor, while the fitting effects of the angle of attack, roll angle, and pitch angle are relatively good, all concentrated near the $y = x$ line.

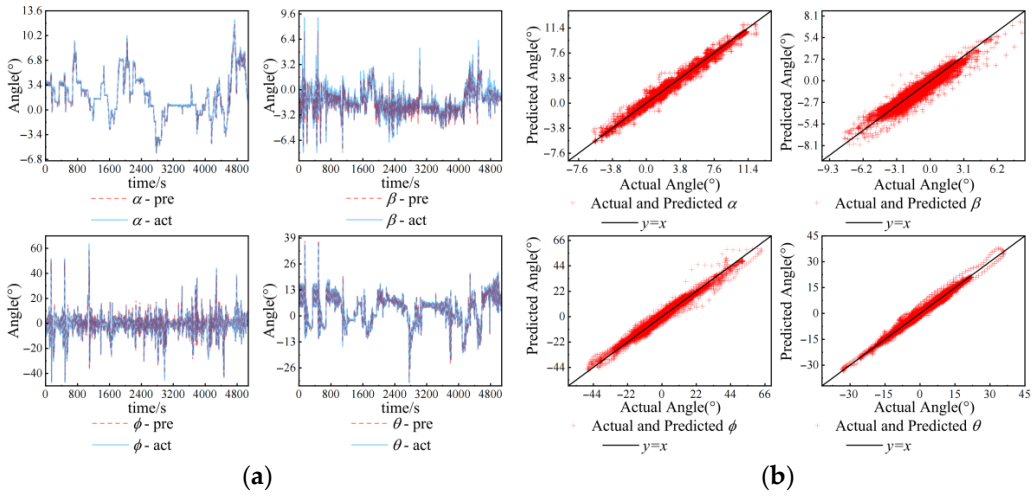


Figure 12. Overall train set results graph of the model: (**a**) time series plot; (**b**) scatter plot of prediction and actual.

The foregoing analysis investigated the prediction outcomes of the model on the training set, which demonstrated high prediction accuracy and good stability. Subsequently, the test set was employed to assess the model's performance on it and examine its generalization capacity.

4.3. Analysis of Model Predictive Results

The quantitative analysis of the results of the aircraft attitude predictive model yields Table 5. It can be observed from the table that for the angle of attack, roll angle, and pitch angle, the prediction accuracy of the model is relatively high, as manifested by the R^2 values close to 1, indicating a small error between the model's predictions and the actual values and that the model can better explain the variability in the data. For the sideslip angle, although the MSE and MAE are relatively small, indicating that the prediction accuracy is acceptable from an engineering perspective because the MAE/MSE fall within the $\pm 1^\circ$ threshold required for flight test safety monitoring, the R^2 value is relatively low, showing weaker statistical fitting performance compared with other attitude parameters. On the whole, the model performs well in predicting attitude angles.

Table 5. Evaluation metrics for model forecast results.

Evaluation Metrics	α	β	φ	θ
MSE	0.126	0.282	3.179	0.756
MAE	0.180	0.421	1.108	0.654
R^2	0.992	0.769	0.982	0.983

When predicting the key attitude parameters of the aircraft-angle of attack, sideslip angle, roll angle, and pitch angle, the overall test set results are shown in Figure 13. The left side is the time series curve of the actual values and predicted values of the test set; the right side is the scatter plot of the actual values and predicted values, with the black solid line being a straight line. The closer the points are to this line, the more accurate the prediction is.

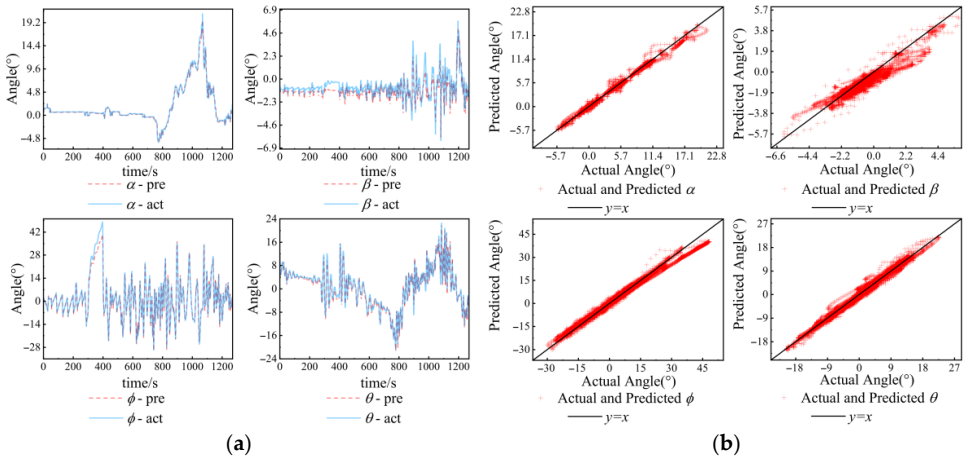


Figure 13. Overall test set results graph of the model: (**a**) time series plot; (**b**) scatter plot of prediction and actual.

On the time series graph, there is a significant deviation between the predicted and actual values during the rapid change in the angle of attack, indicating that the model has limitations in predicting rapid changes in the angle of attack. However, in the scatter plot of the angle of attack, the predicted values and the actual values maintain a good consistency at most data points. On the time series graph, the predictive effect of the sideslip angle is not very ideal, especially in the area where the sideslip angle is small. The scatter plot shows that most of the predictive results are smaller than the actual results.

The scatter plot of the roll angle shows that when the roll angle is greater than 20°, the prediction effect significantly decreases. The possible reason is that the range covered by the training data is relatively small, and there is a lack of training data for larger roll angles. The prediction results of the pitch angle indicate that the model performs well overall in predicting the pitch angle.

The local test set results of the aircraft attitude predictive model are shown in Figure 14. The predictive trends of the roll angle and pitch angle are basically consistent, but there are deviations between the predictive values and the actual values near the extreme points. The predictive values of the angle of attack are basically consistent with the actual values, with high accuracy. The predictive error of the sideslip angle is relatively large, and the predictive effect is not very stable.

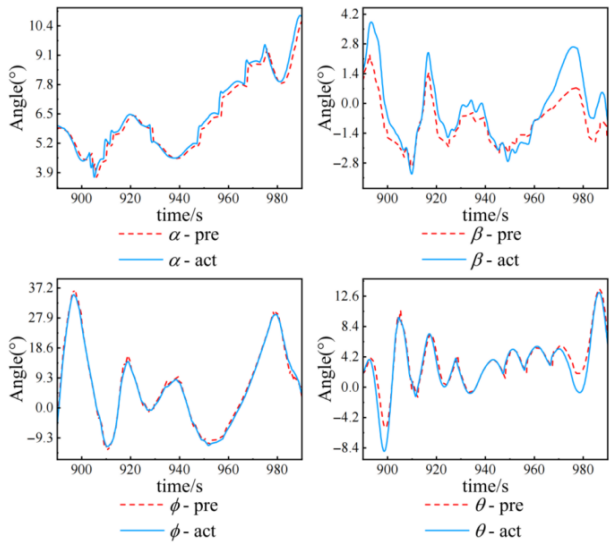


Figure 14. Local test set result diagram of the model.

5. Results and Discussion

5.1. Auxiliary Decision-Making of Angle of Attack Exceeding Limit

Taking the problem of excessive angle of attack as an example, the selected flight segment is shown in Table 6. The pilot's control mainly focuses on the elevator and throttle. Combined with the critical safety attitude parameter threshold Table 2 stored in the knowledge graph in Section 3, it can be seen that the throttle remains unchanged during the selected flight segment. As the deflection angle of the elevator increases, the angle of attack rapidly decreases, even falling below the lower limit of the designed safety knowledge. The angle of attack risk value increases sharply within a short period of time.

Table 6. Time series table of some key parameters during flight.

Time/s	Angle of Attack/°	Elevator/°	Throttle	Risk Value
2772	−3.83	5.75	0.75	1.9
2773	−3.85	5.75	0.75	1.9
2774	−4.77	9.2	0.75	6.7
2775	−5.71	9.2	0.75	8.0

First, focus on the moment when the angle of attack risk value increases sharply, that is, at the 2774th second. Based on the aircraft attitude predictive model and risk quantification method, calculate the current and predicted angle of attack risk value heat map of the manipulation space as shown in Figure 15.

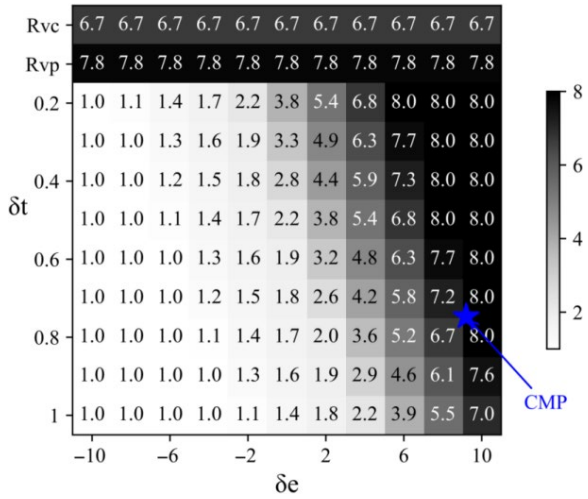


Figure 15. Heat map of current and predicted angle of attack risk value for throttle and longitudinal manipulation space at 2775 s.

The first row in the figure, represented by the letter Rv_c, refers to the angle of attack risk value of the aircraft in its current state. And the second row, represented by the letter Rv_p, refers to the angle of attack risk value of the next second if the aircraft maintains its current control state unchanged. It can be seen that if the current control remains unchanged, the risk of the aircraft's angle of attack exceeding the limit shows a decreasing trend, but it still remains at a relatively high-risk level. The third row and below represent the predicted angle of attack risk values within the selected aircraft manipulation space.

Considering that in the actual control process, except for the aircraft's takeoff and landing process, the deflection angle of the aircraft's control surfaces will not be too large, the selected manipulation space range here is limited. The selected elevator range is [−10, 10] degrees, and the throttle opening is set to [0.2, 1]. The blue star mark in the

figure, which is indicated by the letter CMP, indicates the current position of the elevator and throttle control in the manipulation space. Based on this point's position and the risk value heat map, the correct control direction can be clearly identified. It is easy to see that increasing the throttle and pulling the stick to make the elevator deflect upward can effectively reduce the risk of the angle of attack exceeding the lower limit. From the heat map, it can be seen that the correct control of the elevator is more crucial for reducing the risk value. Returning the elevator to the neutral position can reduce the risk value to a relatively low level, while increasing the throttle at this time has a slightly worse effect; even if the throttle is increased to the maximum, the risk value is still quite large. If the angle of attack risk value does not exceed 4, which is set as the safe range, then the specific safe control range of the throttle and elevator when the angle of attack risk value is in a safe state can be given.

According to Figure 15, reviewing the captured segment Table 6, during the flight process from the 2773rd to the 2774th second, the elevator continued to deflect downward, causing the angle of attack risk value to rise rapidly. At the 2774th second, the elevator was still not manipulated correctly, resulting in the angle of attack exceeding the design lower limit directly in the next moment.

When assisting in decision-making, to present the changes in pilot control and risk values more intuitively, a three-dimensional heat map of the predicted risk of throttle and longitudinal manipulation space angle of attack is Figure 16, mainly including the current and the previous three seconds' time series heat maps, which are updated in real time during safety monitoring. The blue star marks indicate the control points in the manipulation space at the corresponding moment, with the values corresponding to the real-time risk values. The blue triangular marks indicate the throttle opening values that change over time, and within this time period, the throttle opening has almost no change; the blue plus marks indicate the elevator deflection angles that change over time, and as the elevator deflection angle increases, the angle of attack risk value rises sharply. From the three-dimensional heat map, it can be seen how the risk value changes with the manipulation quantity, which is convenient for analyzing the influence of historical manipulation on the risk value.

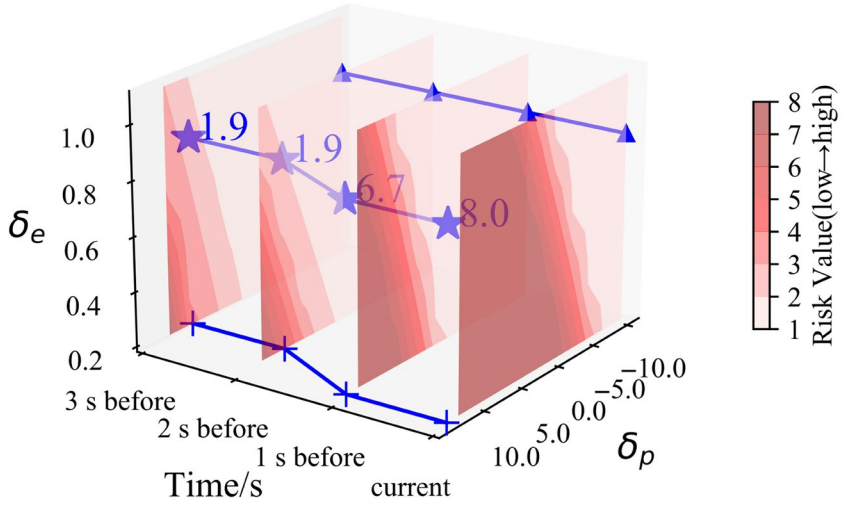


Figure 16. Three-dimensional heat map of timing throttle and longitudinal manipulation space angle of attack prediction risk.

In conclusion, when the aircraft's angle of attack exceeds the lower limit, the correct operation should be to first pull the stick to make the elevator deflect upwards, while simultaneously coordinating an increase in throttle. Similarly, based on the above method,

the correct operation when the angle of attack exceeds the upper limit is to first push the stick to make the elevator deflect downwards, while simultaneously coordinating a reduction in throttle.

5.2. Auxiliary Decision-Making of Sideslip Angle Exceeding Limit

The following is a flight segment excerpt where the sideslip angle exceeded the limit, as shown in Table 7. The sideslip angle limit is [−5, 8] degrees, as indicated in Table 2 of the key safety attitude parameter threshold values in the knowledge graph.

Table 7. Time series table of some key parameters during flight.

Time/s	Sideslip Angle/°	Aileron/°	Rudder/°	Risk Value
6019	−4.24	−0.56	−1.12	1.8
6020	−5.12	−0.56	−1.12	8.0
6021	−5.38	1.83	−1.12	8.0
6022	−4.26	3.33	−1.12	1.9

As shown in Figure 17, it can be seen from the current risk value in the first row that the current sideslip angle risk value is very high, having exceeded the sideslip angle limit. However, the predicted risk value is 1.7, indicating that the current manipulation is correcting the sideslip angle. By maintaining the current manipulation, the aircraft can return to a safe state. Based on the risk value heat map, the specific safety manipulation space for lateral manipulation can be clearly identified. At this time, if rudder manipulation is still needed to turn the aircraft, coordinated manipulation of the ailerons should be used to keep the sideslip angle within a safe level.

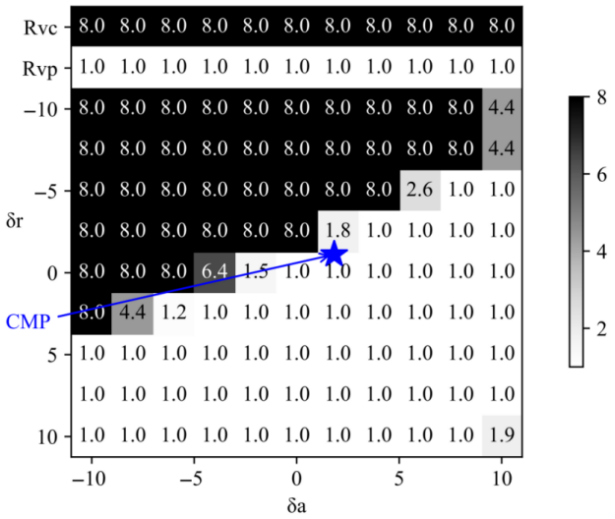


Figure 17. Heat map of current and predicted sideslip angle risk value in lateral manipulation space at 6021 s.

When conducting safety monitoring, Figures 17 and 18 are analyzed and used for decision-making. The time series three-dimensional heat map includes the predictive risk value heat map of the aircraft's manipulation space within the last three seconds. In the three-dimensional heat map, it can be seen that the rudder deflection angle remains almost unchanged. At the beginning, the aileron (left aileron) deflection angle decreases, causing the risk value of the sideslip angle to increase rapidly. In the previous second, the aileron deflection angle is corrected in time, thereby significantly reducing the current risk value of the sideslip angle.

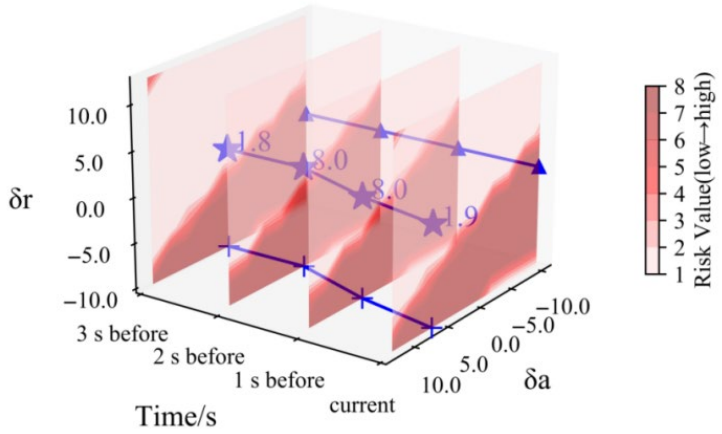


Figure 18. Heat map of current and predicted sideslip angle risk value in lateral manipulation space at 6021 s.

In summary, during safety monitoring, if the aircraft's sideslip angle falls below the lower limit, attention should be paid to lateral manipulation. The ailerons and rudder should be coordinated to manipulate the left aileron to deflect downward and the rudder to deflect to the left. For longitudinal manipulation, the elevator should be adjusted to keep the aircraft level, and the issue of angle of attack exceeding the limit should be noted.

By using the safety manipulation space model to draw the predictive parameter risk heat map within the manipulation space, the magnitude and trend of risks can be clearly identified. Combining the knowledge graph to determine the safety manipulation space can provide reliable decision-making suggestions for pilots. It is also noted that although the 1 s prediction horizon provides meaningful short-term trend estimation, it remains shorter than the 3–5 s lead time typically desired for pilot decision support during abnormal attitude scenarios, which will be addressed in future work.

6. Conclusions

(1) A knowledge graph for flight test safety is constructed, expanding its application scope. By leveraging the depth of knowledge in the flight test safety knowledge graph, the graph not only provides rich background knowledge and parameter support for the aircraft attitude predictive model but also offers scientific manipulation suggestions for flight safety monitoring and decision-making.

(2) A linear risk quantification method is adapted to the flight test safety monitoring context. Compared with the traditional risk interval quantification method, the risk values calculated by this method contain more key information, because the adaptation of this well-established piecewise linear (trapezoidal) mapping technique preserves continuous risk variation, providing more reliable data support for flight test safety monitoring and facilitating more reasonable auxiliary decision-making by safety monitoring personnel.

(3) An aircraft attitude predictive model is built based on neural networks, accurately predicting key aircraft attitude parameters. The average absolute error for the angle of attack prediction is 0.18°. However, the prediction accuracy for the sideslip angle is relatively low and requires further research and improvement. Meanwhile, although this method avoids the impact of data inaccuracies on the results through a data interception mechanism, future research should further explore how to ensure the algorithm's robustness without resorting to data interception. By combining the model's predicted values with the parameter thresholds of the knowledge graph and using the risk quantification method, the aircraft's safety manipulation space is calculated. Through a visual display design, these key pieces of information are made more intuitive and understandable. This not only provides a

theoretical basis for pilots' operation decisions in abnormal attitude situations but also offers new technical means and practical guidance for the field of flight safety.

Author Contributions: Conceptualization, Z.Y.; Data curation, Z.Y.; Writing—original draft, Z.Y.; Methodology, Z.Y.; Investigation, S.H.; Validation, S.H.; Formal analysis, S.H.; Writing—review and editing, S.H., Y.Z., and W.Y.; Method process, Y.Z. and W.Y.; Thesis Proofreading, Y.Z. and W.Y.; Project administration, Y.Z.; Funding acquisition, W.Y. All authors have read and agreed to the published version of the manuscript.

Funding: This research was supported by the Key Technologies of Typical Special Test Flight of Civil Aircraft (Project No. MJZ5-1N22).

Data Availability Statement: The data that support the findings of this study are available from the corresponding author upon reasonable request.

Conflicts of Interest: The authors declare no conflicts of interest.

References

1. Zolghadri, A. A review of fault management issues in aircraft systems: Current status and future directions. *Prog. Aerosp. Sci.* **2024**, *147*, 101008. [CrossRef]
2. Abu-Salih, B. Domain-specific knowledge graphs: A survey. *J. Netw. Comput. Appl.* **2021**, *185*, 103076. [CrossRef]
3. Tian, L.; Zhou, X.; Wu, Y.-P.; Zhou, W.-T.; Zhang, J.-H.; Zhang, T.-S. Knowledge graph and knowledge reasoning: A systematic review. *J. Electron. Sci. Technol.* **2022**, *20*, 100159. [CrossRef]
4. Lopez, V.; Hoang, L.; Martinez-Galindo, M.; Fernández-Díaz, R.; Sbodio, M.L.; Ordonez-Hurtado, R.; Zayats, M.; Mulligan, N.; Bettencourt-Silva, J. Enhancing foundation models for scientific discovery via multimodal knowledge graph representations. *J. Web Semant.* **2023**, *84*, 100845. [CrossRef]
5. Zhou, D.; Zhuang, X.; Zuo, H.; Cai, J.; Zhao, X.; Xiang, J. A model fusion strategy for identifying aircraft risk using CNN and At t-BiLSTM. *Reliab. Eng. Syst. Saf.* **2022**, *228*, 108750. [CrossRef]
6. Raju, S.; Pingali, P.; Varma, V. An Unsupervised Approach to Product Attribute Extraction. *DBLP* **2009**, *5478*, 796–800.
7. Chen, C.; Wang, T.; Zheng, Y.; Liu, Y.; Xie, H.; Deng, J.; Cheng, L. Reinforcement learning-based distant supervision relation extraction f or fault diagnosis knowledge graph construction under industry 4.0. *Adv. Eng. Inform.* **2023**, *55*, 101900. [CrossRef]
8. Li, Z.; Ding, N.; Liang, C.; Cao, S.; Zhai, M.; Huang, R.; Zhang, Z.; Hu, B. A semi-supervised framework fusing multiple information for knowledge graph entity alignment. *Expert Syst. Appl.* **2024**, *259*, 125282. [CrossRef]
9. Munne, R.F.; Ichise, R. Entity alignment via summary and attribute embeddings. *Log. J. IGPL* **2023**, *31*, 314–324. [CrossRef]
10. Qian, Y.; Pan, L. Leveraging multimodal features for knowledge graph entity alignment based on dynamic self-attention networks. *Expert Syst. Appl.* **2023**, *228*, 120363. [CrossRef]
11. Xiong, M.; Wang, H.; Wong, Y.D.; Hou, Z. Enhancing aviation safety and mitigating accidents: A study on aviation safety hazard identification. *Adv. Eng. Inform.* **2024**, *62*, 102732. [CrossRef]
12. Liang, X.; Wang, Z.; Li, M.; Yan, Z. A survey of LLM-augmented knowledge graph construction and application in complex product design. *Procedia CIRP* **2024**, *128*, 870–875. [CrossRef]
13. Fan, Y.; Sun, Y.; Mi, B. Flight Control System Knowledge Graph Construction Based On Aeronautical Domain Knowledge Augmented Large Language Model. In Proceedings of the 34th Congress of the International Council of the Aeronautical Sciences, Florence, Italy, 9–13 September 2024.
14. Huang, C. Applying Knowledge Discovery Process in General Aviation Flight Performance Analysis. *Trends Tech. Sci. Res.* **2020**, *4*, 555633. [CrossRef]
15. Dagdelen, J.; Dunn, A.; Lee, S.; Walker, N.; Rosen, A.S.; Ceder, G.; Persson, K.A.; Jain, A. Structured information extraction from scientific text with large language models. *Nat. Commun.* **2024**, *15*, 1418. [CrossRef] [PubMed]
16. Qu, J.; Wang, J.; Zhao, Z.; Chen, X. Remote supervised relationship extraction method of clustering for knowledge graph in aviation field. *Intell. Syst. Appl.* **2024**, *22*, 200377. [CrossRef]
17. Xiong, H.; Wang, S.; Tang, M.; Wang, L.; Lin, X. Knowledge Graph Question Answering with semantic oriented fusion model. *Knowl. Based Syst.* **2021**, *221*, 106954. [CrossRef]
18. Zhu, S.; Cheng, X.; Su, S. Knowledge-based question answering by tree-to-sequence learning. *Neurocomputing* **2020**, *372*, 64–72. [CrossRef]
19. Zhang, J.-C.; Zain, A.M.; Zhou, K.-Q.; Chen, X.; Zhang, R.-M. A review of recommender systems based on knowledge graph embedding. *Expert Syst. Appl.* **2024**, *250*, 123876. [CrossRef]

20. Gómez-Romero, J.; Molina-Solana, M.; Oehmichen, A.; Guo, Y. Visualizing large knowledge graphs: A performance analysis. *Future Gener. Comput. Syst.* **2018**, *89*, 224–238. [CrossRef]
21. Xu, C.; Fu, C.; Liu, W.; Sheng, S.; Yang, S. Data-driven decision model based on dynamical classifier selection. *Knowl. Based Syst.* **2020**, *212*, 106590. [CrossRef]
22. Lu, Y.; Zhang, S.; Zhang, Z.; Zhang, X.; Tang, P.; Fu, S. Multiple hierarchy risk assessment with hybrid model for safety enhancing of unmanned subscale BWB demonstrator flight test. *Chin. J. Aeronaut.* **2019**, *32*, 2612–2626. [CrossRef]
23. Shi, Z.; Pan, Q.; Xu, M. LSTM-Cubic A*-based auxiliary decision support system in air traffic management. *Neurocomputing* **2020**, *391*, 167–176. [CrossRef]
24. Su, C.; Jiang, Q.; Han, Y.; Wang, T.; He, Q. Knowledge graph-driven decision support for manufacturing process: A graph neural network-based knowledge reasoning approach. *Adv. Eng. Inform.* **2025**, *64*, 103098. [CrossRef]
25. Atoui, M.A.; Cohen, A. Coupling data-driven and model-based methods to improve fault diagnosis. *Comput. Ind.* **2021**, *128*, 103401. [CrossRef]
26. Djeumou, F.; Neary, C.; Goubault, E.; Putot, S.; Topcu, U. Neural Networks with Physics-Informed Architectures and Constraints for Dynamical Systems Modeling. *Learn. Dyn. Control. Conf.* **2021**, *168*, 263–277.
27. Wang, G.; Pei, B.; Xu, H.; Lv, M.; Zhao, Z.; Bu, X. Risk Quantification and Visualization Method for Loss-of-Control Scenarios in Flight. *Aerospace* **2023**, *10*, 416. [CrossRef]
28. Hamza, M.H.; Polichshuk, R.; Lee, H.; Parker, P.; Campbell, A.; Chattopadhyay, A. Aircraft post-upset flight risk region prediction for aviation safety management. *Adv. Eng. Inform.* **2022**, *54*, 101804. [CrossRef]
29. Ding, D.; Wang, Q.; Chen, Q.; He, L. Symbolic Regression-Based Modeling for Aerodynamic Ground-to-Flight Deviation Laws of Aerospace Vehicles. *Aerospace* **2025**, *12*, 455. [CrossRef]
30. Rubio-Hervas, J.; Gupta, A.; Ong, Y.-S. Data-driven risk assessment and multicriteria optimization of UAV operations. *Aerosp. Sci. Technol.* **2018**, *77*, 510–523. [CrossRef]
31. Li, C.; Sun, R.; Pan, X. Takeoff runway overrun risk assessment in aviation safety based on hum an pilot behavioral characteristics from real flight data. *Saf. Sci.* **2023**, *158*, 105992. [CrossRef]
32. Reiser, C.; Villani, E.; Machado Cardoso-Junior, M. A novel approach to runway overrun risk assessment using FRAM and flight data monitoring. *Aeronaut. J.* **2024**, *128*, 2054–2072. [CrossRef]
33. Wang, G.; Xu, H.; Pei, B. An intelligent approach for flight risk prediction under icing conditions. *Chin. J. Aeronaut.* **2023**, *36*, 109–127. [CrossRef]
34. Babl, M.L.D.; Engelbrecht, J.A.A. Automatic Deep Stall Recovery using Optimal Trajectory Planning. *IFAC-PapersOnLine* **2020**, *53*, 15508–15515. [CrossRef]
35. Grillo, A.; Torre, G.; Bunge, R. Optimal Stall Recovery via Deep Reinforcement Learning for a General Aviation Aircraft. In Proceedings of the AIAA SCITECH 2024 Forum, Orlando, FL, USA, 8–12 January 2024.
36. Sekimoto, S.; Kato, H.; Fujii, K.; Yoneda, H. In-Flight Demonstration of Stall Improvement Using a Plasma Actuator for a Small Unmanned Aerial Vehicle. *Aerospace* **2022**, *9*, 144. [CrossRef]

Disclaimer/Publisher's Note: The statements, opinions and data contained in all publications are solely those of the individual author(s) and contributor(s) and not of MDPI and/or the editor(s). MDPI and/or the editor(s) disclaim responsibility for any injury to people or property resulting from any ideas, methods, instructions or products referred to in the content.